Comparative study on oxidation behavior of Ti$_2$AlN coatings in air and pure steam

Zhenyu Wang[a], Xiaowei Li[a,c], Wentao Li[a], Peiling Ke[a,b,*], Aiying Wang[a,b,**]

[a] Key Laboratory of Marine Materials and Related Technologies, Zhejiang Key Laboratory of Marine Materials and Protective Technologies, Ningbo Institute of Materials Technology and Engineering, Chinese Academy of Sciences, Ningbo, 315201, China
[b] Center of Materials Science and Optoelectronics Engineering, University of Chinese Academy of Sciences, Beijing, 10049, China
[c] Computational Science Center, Korea Institute of Science and Technology, Seoul, 136-791, Republic of Korea

A B S T R A C T

The oxidation behavior of the Ti$_2$AlN coatings is comparatively investigated at 750 °C in air and in pure steam conditions, respectively. The linear kinetics composed of two stages is observed for each case, suggesting a chemical reaction determining process, and the second stage behaves a slightly higher oxidation rate. In air, the oxidation behavior exhibits an inhomogeneous oxidation due to the presence of macro-particles and impurity phases in the coating, while a transition from inhomogeneous oxidation to homogeneous oxidation occurs in pure steam. Compared to that in air, the oxidation process in pure steam is accelerated, leading to higher mass gains. XRD and EDX analyses indicate that Al easily diffuses to the surface and thus forms α-Al$_2$O$_3$ layer under the two atmospheres, which result from the high Al activity within MAX phase. Additionally, the scaling mechanism of Ti$_2$AlN coatings is discussed in terms of the microstructure evolution.

1. Introduction

Ti$_2$AlN belongs to one of the novel ternary nanolaminated compounds with the general formula M$_{n+1}$AX$_n$, abbreviated as MAX phase, where M is an early transition metal, A is a group 13–16 element, and X is carbon and/or nitrogen. It has been gained wide attention due to its interesting properties combining those of ceramics and metals, such as good electrical and thermal conductivity, high-temperature capability, easy machinability, excellent thermal shock resistance, as well as superior oxidation and corrosion resistances etc. [1,2]. These superior properties make Ti$_2$AlN of particular interest as protective coatings for middle/high-temperature applications [3–5].

Many efforts [3,6,7] have been performed on Ti$_2$AlN or other Al-based MAX phase materials, including bulk and coating forms, and revealed that in most Al-based MAX phase bulk materials the excellent oxidation-resistant property can be attributed to the continuous and dense Al$_2$O$_3$ layer forming on the specimen surface. Besides, the Al$_2$O$_3$ layer also possessed good compatibility with the MAX phase, resulting from the small differences of their thermal expansion coefficient, which could protect the underlying MAX phase against further oxidation

attack at high temperature [8,9]. Generally, the oxidation kinetics of MAX phase followed parabolic law [10–12]. Li et al. [13] studied the oxidation resistance of Cr$_2$AlC coatings prepared using magnetron sputtering, and found that the oxidation rate of the Cr$_2$AlC coating was rather lower than that of Ni-based superalloy M38G at 900–1100 °C in air. Wang et al. [14] showed that the Cr$_2$AlC-coated specimens exhibited much better oxidation resistance in contrast to the bare alloy for isothermal oxidation processes at 700 °C and 800 °C in air. However, it was reported that the MAX phase coatings suffered more serious oxidation than that of the bulk materials because of their limited coating thickness and Al content, columnar structure, and the existence of other impurity phases, etc. [13–15].

On the other hand, most of previous studies about the oxidation behavior of MAX phase focused on air condition. In many energy related systems such as coal-fired and nuclear power plant, pure steam is a typical environmental condition. Especially, in order to improve the thermal efficiency, the steam parameters including temperature and pressure increase significantly year by year, which cause the corresponding steam oxidation becoming a more concerning problem. Therefore, exploring the steam oxidation mechanism is of crucial

---

importance for both scientific understanding and engineering application [16,17]. Zhou et al. [18] studied the role of steam on the oxidation of Ti_3AlC_2 and Ti_2AlC bulk materials at 500–1200 °C in controlled humidity atmospheres, and observed that the breakaway oxidation took place at 500–600 °C as the steam induced cracks in the oxide scales and failed to form a protective Al_2O_3 scale; at elevated temperatures, the steam slightly accelerated the oxidation of Ti_2AlC due to the enhanced ion transportation pathway by increasing the oxygen vacancy. Simulated Loss of Coolant Accident (LOCA) tests in nuclear system performed at 1005 °C presented that Ti_2AlC coatings provided efficient protection for the underlying Zry-4 [19]. Feng et al. [5] reported that there was no distinct layered oxide scale observed on the Ti_2AlC coatings after 200 h oxidation in pure steam. However, compared to air oxidation, the oxidation mechanism of MAX phase coatings in pure steam is still not fully clarified yet. Up to now, as we known, the oxidation behavior and oxidation mechanism of Ti_2AlN coating in pure steam have never been reported before. Hence, a comprehensive understanding of pure steam effects on the oxidation processes of Ti_2AlN coatings is important for its wide applications in harsh nuclear systems particularly.

In the previous work [20], we have fabricated the dense, columnar structure-free, and high-stability Ti_2AlN coatings on Ti−6Al−4V (TC4) alloys by using a combined cathodic arc/sputter deposition approach, followed by a vacuum heat treatment. In this paper, the systematic oxidation behaviors of the obtained Ti_2AlN coatings in air and pure steam were investigated comparatively, and the corresponding oxidation mechanism was discussed in terms of the structural evolution during the oxidation process. To sufficiently meet the requirement of harsh working temperature and accelerate the oxidation process, a relatively high oxidation temperature of 750 °C was selected in this study. The aim of this study was to shed light on the role of steam on the oxidation behavior of Ti_2AlN MAX phase coatings.

2. Experimental details

The Ti_2AlN coatings were deposited on the mirror-polished Ti−6Al−4V (TC4) alloy substrate by the combined cathodic arc/sputter technology, followed by heat post-treatment in this study. The nominal composition of this alloy in weight per cent is: Al, 6.04; V, 4.03; Fe, 0.3; O, 0.1; N, 0.05; H, 0.015 and the balance Ti. The circular titanium target (Φ128 mm × 15 mm, purity of 99.9%) and the rectangular aluminum target (400 mm × 100 mm × 7 mm, purity of 99.9%) were used as arc cathode source and sputtering source, respectively. A schematic diagram of the combined deposition system was illustrated in Fig. 1. Gas mixtures of Ar and N_2 with the pressure of 2.0 Pa were used as reactive gas sources, where the flowing ratio of N_2 to Ar was set to 1/10. To ensure all the substrate faces were coated, the substrates were fixed at the front of Al target with a distance of 5 cm to the target in a hanging position. Prior to deposition, the TiN diffusion barrier about
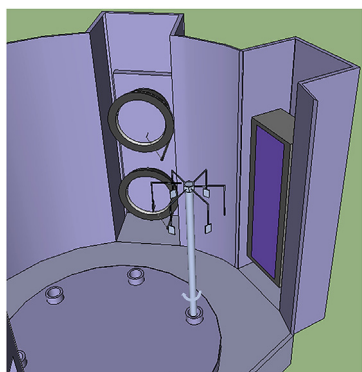
Fig. 1. Schematic diagrams of the coating deposition system.
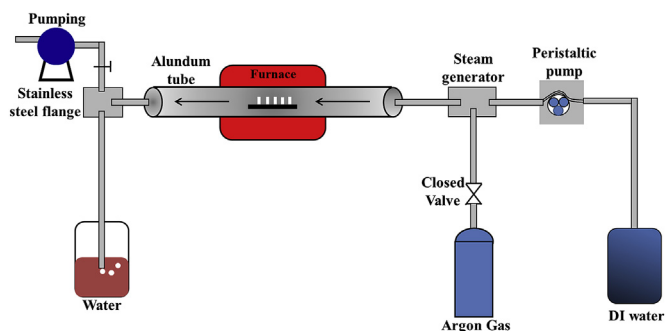
Fig. 2. Schematic diagrams of the oxidation system.

600 nm was prepared to prevent inter-diffusion of elements between the coating and substrates in later thermal treatment process. During deposition, Ti target power and Al target power were controlled at 18 W and 3.1 kW, respectively, with the deposition temperature of 200 °C. Then, annealing treatment of the as-deposited Ti−Al−N coating was conducted at 800 °C in vacuum for 1.5 h. Before annealing, the vacuum degree was set to 1.0×10^{-2} Pa. The detailed preparation process, surface and cross-sectional backscatter morphologies as well as the XRD results could be found in our previous published paper [20]. The sizes of the coated samples and the blank substrates were all fixed at 20 × 10 × 3 mm. Quantitative analysis revealed that the annealed coatings are composed of three phases: dominant Ti_2AlN phase (81.7 wt %), TiN (16.2 wt%) and $TiAl_x$ (2.1 wt%) [20].

Intermittent isothermal oxidation tests were conducted in static air and flowing steam atmosphere at 750 °C in alumina crucibles placed in a tube furnace (see Fig. 2). Flowing steam was made by pumping deionized water into the preheating steam generator at a fixed rate of 1 ml/min. When the furnace temperature increased to 750 °C, the furnace was pumped to 10 Pa and then the preheated steam was introduced immediately. After oxidation, the flowing steam was cut off and the oxidation specimens were taken out of the furnace, and cooled down to room temperature at various intervals for mass change measurement. The total mass of the oxidized specimen along with the crucible was recorded. The sensitivity of the balance used for the mass measurement was 10^{-5} g. For comparison, oxidation exposures of the coatings in static air were performed in the same tube furnace and the same mass measuring method was used.

Phase identifications of the Ti_2AlN coatings after oxidation tests were determined by XRD (D8-Advance Brucker, Cu Ka) and Raman (Renishaw inVia, 532 nm). The overview morphologies and chemical composition of the scales were assessed by using SEM (FEI Quanta FEG 250, 15 kV) and EDX (Oxford, 15 kV). To avoid the effects of mechanical polishing on the results, cross-section samples were prepared by means of a Broad Ion Beam (BIB) instrument (Leica EMTIC 3X). The milling voltage was 6 kV and milling time was about 3 h, respectively.

3. Results

3.1. Oxidation kinetics

Fig. 3 shows the measured oxidation kinetic curves of the TC4 substrates without and with the Ti_2AlN coatings. A linear growth rule for the bare TC4 substrates is observed for both air and steam oxidations. However, noted that the Ti_2AlN coatings also exhibit a linear growth rule during oxidation in the both atmospheres, suggesting that the mass gains of the coated specimens are controlled by the oxidizing reaction rather than the diffusion. The linear rate constants are modeled by the following equation:

$$k_p = \frac{\Delta w / A}{t} \tag{1}$$
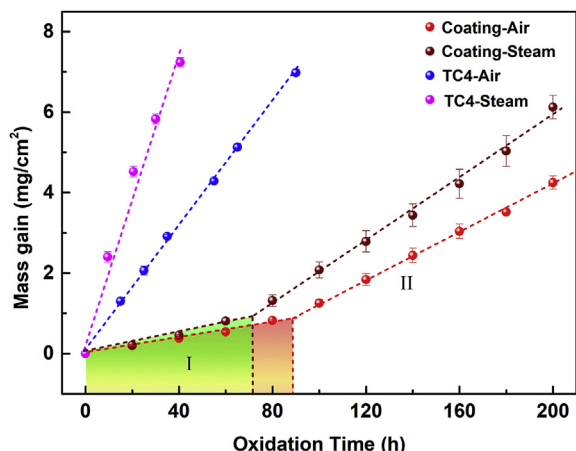
Fig. 3. Oxidation kinetics of the Ti$_2$AlN coatings and TC4 substrates in air and pure steam.

Table 1
Summary of rate constants.

	TC4		T2AlN coatings			
	k_p (g/cm^2·s)	R^2	I		II	
			k_p (g/cm^2·s)	R^2	k_p (g/cm^2·s)	R^2
O$_2$	2.11×10^{-5}	0.99	2.5×10^{-6}	0.99	7.78×10^{-6}	0.99
H$_2$O	4.44×10^{-5}	0.98	3.61×10^{-6}	0.99	1.06×10^{-5}	0.99

where k$_p$ is the linear rate constant (g/cm^2/s), Δw/A is the mass gain per unit area (g/cm^2) and t is the oxidation time (s). All the calculated rate constants are listed in Table 1, where the R^2 approaching 1 suggests good fitting quality. The oxidation kinetics divided into two stages (marked by 'I' and 'II', respectively, in Fig. 3) is clearly distinguished, and the transition points are identified at ∼70 h in air and ∼90 h in steam, respectively. The oxidation rates in the second stage, which are 7.78×10^{-6} g/cm^2·h in air and 1.06×10^{-5} g/cm^2·h in pure steam, separately, are higher than that of the first stage, indicating the occurrence of a more serious oxidation process. Meanwhile, the oxidation kinetics in pure steam is higher than that in air during the two stages, underlying that steam slightly accelerates the oxidation process of Ti$_2$AlN coatings. However, compared to the bare substrates (6.98 g/cm^2 after 90 h in air and 6.13 g/cm^2 after 40 h in pure steam), the coated specimens exhibit much lower weight gains, which are 4.25 g/cm^2 in air and 6.13 g/cm^2 in pure steam, respectively, after 200 h. This implies that the oxidation resistance of bare TC4 substrates can be significantly enhanced by introducing the Ti$_2$AlN coatings.

3.2. Oxidation results in air

3.2.1. Characterization of the oxidation products

Fig. 4 shows the XRD patterns of Ti$_2$AlN coatings after oxidation in air for 20, 60, 160 and 200 h separately. The intensity of diffraction peaks corresponding to Ti$_2$AlN and TiN phases decreases with increasing oxidation time, suggesting that the Ti$_2$AlN and TiN phases are gradually oxidized during oxidation. In the case of 20 h oxidation, only X-ray peaks of rutile-TiO$_2$ are detected, and no other peaks of oxides, such as anatase-TiO$_2$ or α-Al$_2$O$_3$, appear in the XRD patterns, because these products are amorphous or weak crystalline state. With further increasing oxidation time to 160 h, the diffraction peaks of α-Al$_2$O$_3$ exist. In addition, the diffraction peak of Ti$_2$AlN is clearly distinguished after 200 h, implying that the Ti$_2$AlN coatings provide further protection for the TC4 alloys. To understand the oxide scale feature, Raman spectrum analysis is performed at various oxidation times. As shown in
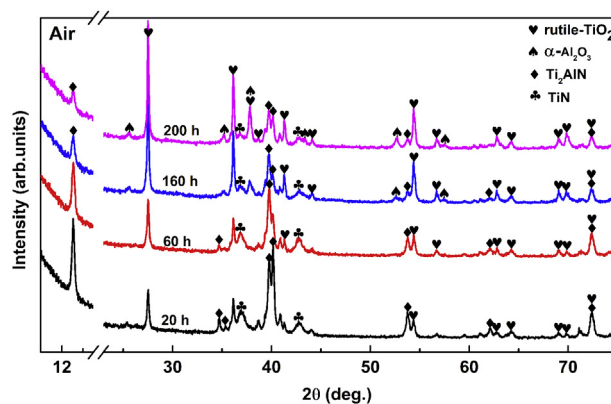
Fig. 4. XRD patterns for the oxide scales formed on the Ti$_2$AlN coatings in air after 20 h, 60 h, 160 h and 200 h.
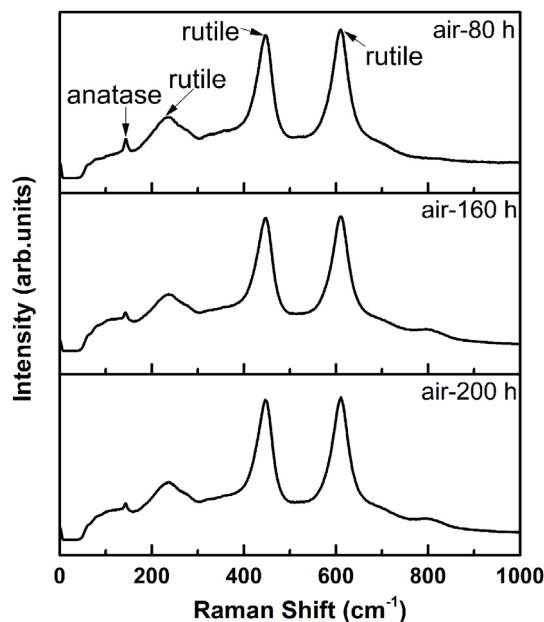
Fig. 5. Raman patterns for the oxide scales formed on the Ti$_2$AlN coatings in air at 750 °C after 80 h, 160 h and 200 h.

Fig. 5, the strongest band at 145 cm^{-1} is assigned to the characteristic peak of anatase-TiO$_2$, and the Raman shifts at 447 and 610 cm^{-1} are related to those of rutile-TiO$_2$. Hence, the above Raman analysis reveals that the TiO$_2$ oxide products are a mixture of anatase and rutile phase, but mainly rutile phase.

3.2.2. Microstructural evolution of the Ti$_2$AlN coatings during oxidation

To understand the microstructural evolution of the Ti$_2$AlN coatings during oxidation, both the plan views and cross-section morphologies of samples after different oxidation times are studied using SEM. Fig. 6 gives typical surface morphologies after oxidation time ranged from 20 h to 200 h. After 20 h oxidation (Fig. 6a), small oxide grains are formed at the large macro-particles, where are enriched in Ti. Combined with the XRD results, it confirms that these oxide products are mainly TiO$_2$ (rutile). In addition, Ti oxides are known to grow rapidly and cannot provide adequate protection above 600–700 °C. However, the oxide growth is nearly invisible in the areas free of macro-particles under the limited resolution of the SEM. After 80 h oxidation, the fine oxide grains (arrowed in Fig. 6c) appear, and then grow up and gather together with increasing the oxidation time. Nevertheless, the oxides do not completely cover over the coating, suggesting that it can further provide protection for the substrates. Above all, we can conclude that
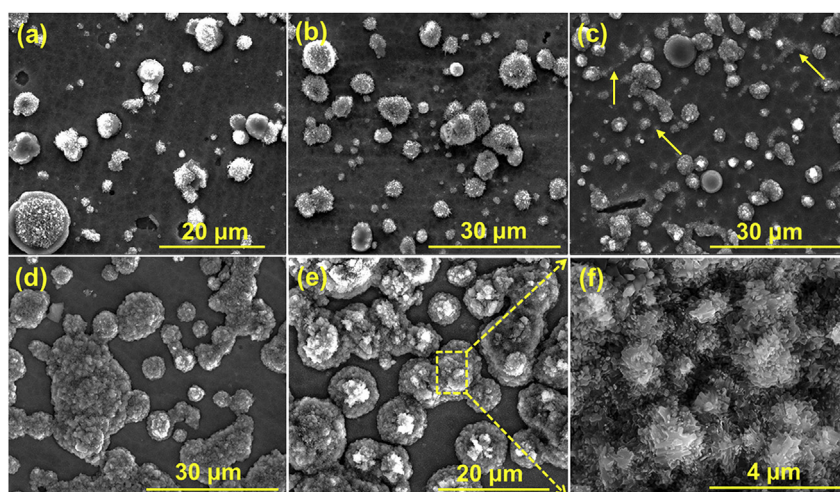
Fig. 6. Surface morphologies for the oxide scales formed on the Ti$_2$AlN coatings in air at 750 °C after (a) 20 h, (b) 60 h, (c) 80 h, (d) 160 h, (e) 200 h and (f) the enlarged view of the square in (e).

the obvious inflection in the mass gain is mainly related to the formation of fine oxide grains in the areas free of macro-particles. An enlarged view of the oxide product in Fig. 6e is shown in Fig. 6f, in which the oxides exhibit a dense structure.

In order to determine the composition of the oxides and diffusion behavior of elements, EDS test is conducted. According to our previous studies [20], the Ti/Al atomic ratio was close to 3:1 for the coating and Ti was especially enriched in macro-particles. After 20 h oxidation, the Ti/Al atomic ratio decreases to 1.91 in the areas free of macro-particles (marked as spots 2) and 1.56 in the oxide areas (marked as spots 1), respectively, suggesting the diffusion of Al to the surface during oxidation. After 200 h, the Ti/Al atomic ratio decreases to 1.26 in oxide gathering areas, instead it increases to 2.17 in other areas, revealing that more Al diffuse to the surface along the oxides to form Al$_2$O$_3$. Although EDS is not the most reliable tool for quantification of O and N, we can still see the tendencies of elements variation. EDS analyses reveal the presence of more than 64 at.% and 47 at.% O content on the oxide gathering areas and coating surface. After 200 h oxidation, compared to 20 h, a 7 at.% increase in amount of oxygen is observed while the nitrogen content decreases by 5 at.%, demonstrating that the coating is gradually oxidized. EDS mapping analysis of the Ti, Al and O elements (Fig. 7 d-f) from the entire surface confirms that Al and O are enriched in the oxides. Furthermore, this phenomenon is more prominent after 200 h, as shown in Fig. 8d–f. The layer feature of oxides is form after 20 h oxidation, which can be ascribed to the presence of defects and cracks at the oxides, providing more channels for rapid diffusion of Al and O. The high activity of Al in the Ti$_2$AlN MAX phase will promote this process.

Typical cross-section morphologies of the scales are formed on the coating surface after 60 h and 160 h oxidation are presented in Figs. 9 and 10, respectively. The oxide bumps, corresponding to the oxide gathering area, are distributed over the coating. Moreover, according to the different contrast of backscattered SEM surface image from the outer layer to inner layer, the layered structure is obvious in these regions for oxide bumps, as shown in Fig. 9a. The EDS line scanning profiles and EDS mapping, as shown in Fig. 9b, c and d, are adopted to further investigate the layer structure of the bumps and the formation of the thin oxide layer in the areas free of bumps. The outer layer is enriched in Al and O, while the inner layer is enriched in Ti and O, which are in agreement with the surface EDS results. Combined with the XRD results, it can be concluded that in the oxide bumps a double structure is generated, in which the outer layer is mainly composed of α-Al$_2$O$_3$ and the inner layer is dominated by TiO$_2$. After 160 h oxidation, the bumps grow up and the layer feature becomes more distinct, as

shown in Fig. 10a, when the bumps with dense structure form in air consist of three layers. EDS mapping (Fig. 10d) and chemical composition of the points (Table 3, point 3–7) reveal that both the outer and inner layers are composed of the TiO$_2$ and Al$_2$O$_3$ mixed oxides, but the outer layer is mainly contributed by Al$_2$O$_3$, and the inner layer mainly consists of TiO$_2$. Meanwhile, the middle layer composed of TiO$_2$ is identified.

EDS line-scanning profiles are shown in Fig. 9b. The peaks of Al and O are clearly identified in the coating surface. Meanwhile, Ti content decreases from the inside of coating to the surface, and a faint Ti peak is observed, indicating that the thin scale composed of Al$_2$O$_3$ and TiO$_2$ is formed on the coating surface. Thus, the thickness of this thin oxide layer has no significant increase after 160 h (Fig. 10b) as a result of the dense structure of the coatings, which effectively prevents the diffusion of O^{2-} and other metal ions. In addition, the peak of Al concentration decreases from the coatings to the coating/substrate interface for both 60 h and 160 h oxidation, which implies that the internal diffusion of Al into the substrate occurs and the thickness of the diffusion layer is about 8 μm. Meanwhile, the enrichment of Ti at the coating/substrate interface is also observed in Fig. 10b, suggesting that the outward diffusion of Ti atoms occurs after 160 h oxidation in air. The point chemical analysis (point 2, 3, 4 in Table 2 and point 9, 10 in Table 3) confirms the presence of the diffused behavior. Therefore, an appropriate diffusion barrier should be applied at the coating/substrate interface against the thermal diffusion of Al.

3.3. Oxidation results in pure steam

3.3.1. Characterization of the oxidation products

XRD patterns of the coatings after oxidation in pure steam at 20, 80, 140 and 200 h are shown in Fig. 11. It is found that TiO$_2$ with the rutile structure starts to be evolved after 20 h oxidation, but its relative intensity is lower than that in air. This is because the nucleation or growth rate of TiO$_2$ is slower in pure steam than in air at the initial stage of oxidation. In addition to rutile phase, anatase phase is observed to be formed at 80 h. Lee and Park [21] investigated the low-temperature oxidation behavior of metallic Ti films in dry and wet air atmospheres, respectively, and found that the anatase-phase TiO$_2$ formed in wet atmosphere. However, α-Al$_2$O$_3$ is initially detected in the scale after 140 h, and the intensity of α-Al$_2$O$_3$ peak increases with prolonging oxidation time. The α-Al$_2$O$_3$ or other alumina phases, e.g. γ-Al$_2$O$_3$ and θ-Al$_2$O$_3$, may form earlier than 140 h, but no obvious crystalline peaks are visible within the XRD resolution limits. The diffraction peaks of both the Ti$_2$AlN and TiN phases are nearly vanished after 200 h,
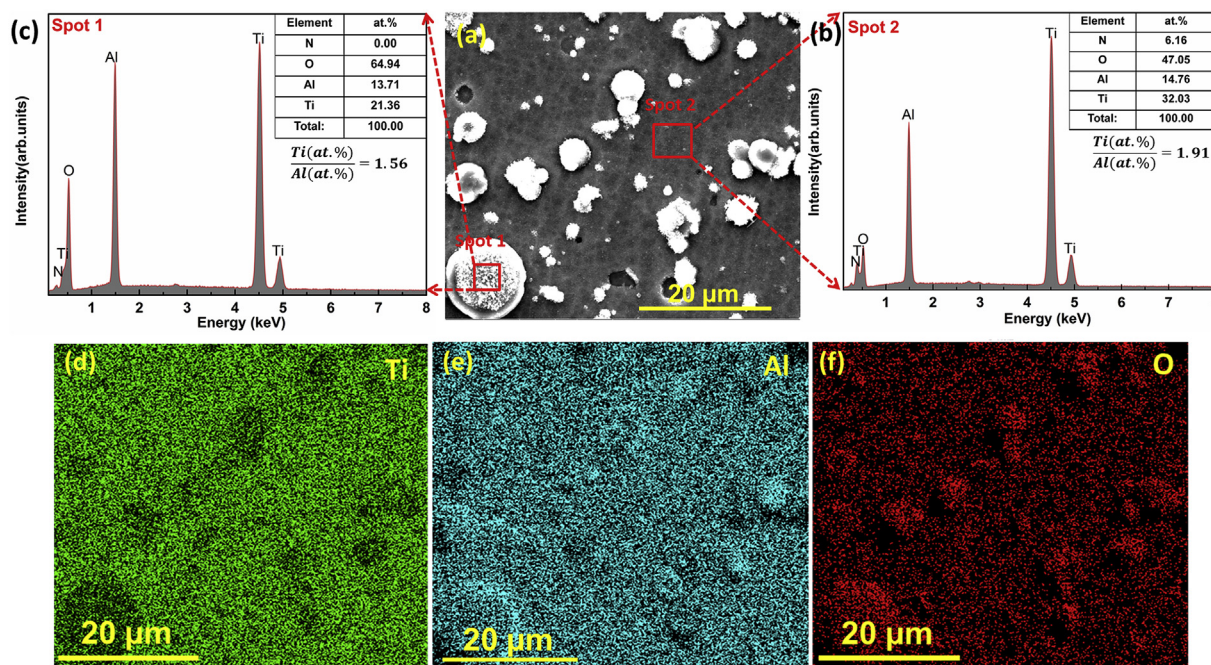
Fig. 7. (a) Surface morphologies for the oxide scales formed on the Ti$_2$AlN coatings in air at 750 °C after 20 h, (b) chemical composition of the spot2 marked in (a), (c) chemical composition of the spot1 marked in (a), (d) Ti, (e) Al, and (f) O elements mapping.

indicating that the coatings suffer more severe oxidation in pure steam compared to that in air. Fig. 12 shows the Raman spectra of the scales after oxidation for 80 h, 140 h and 200 h in pure steam. The sharp and strong band at 145 cm^{-1} is assigned to the characteristic peak of anatase; and the Raman shifts at 447 and 610 cm^{-1} are related to those of rutile. Compared to anatase, rutile is a more stable polymorph at high temperature. Therefore, the anatase gradually transforms to rutile with increasing the oxidation time, and after 200 h, most anatase transforms to rutile in the oxide scale.

3.3.2. Microstructural evolution during Ti$_2$AlN coatings oxidation

Fig. 13 shows the surface morphologies evolution of the scale in pure steam. In line with the air oxidation, after 20 h oxidation (Fig. 13a), small oxidation grains are initially formed on the macro-particles and the thin oxide layer appears in the areas free of macro-particles, but it is difficult to be detected under the limited resolution of the SEM. After 60 h, many needle-like oxides begin to emerge in the areas free of macro-particles. The reason for this is most probably that the oxidation kinetics curves reach to the second stage at about 60 h, earlier 20 h than in air. Unlike air oxidation, the surface of the oxidized coatings is covered completely by the oxides after 80 h in steam,
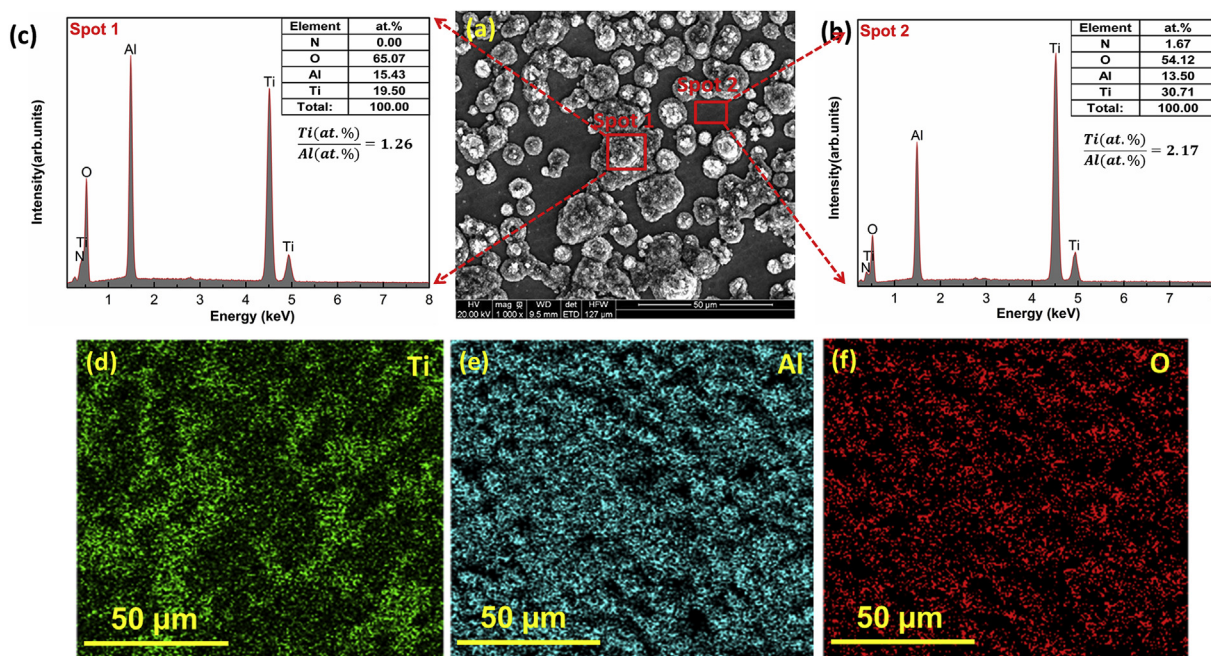
Fig. 8. (a) Surface morphologies for the oxide scales formed on the Ti$_2$AlN coatings in air at 750 °C after 200 h, (b) chemical composition of the spot2 marked in (a), (c) chemical composition of the spot1 marked in (a), (d) Ti, (e) Al, and (f) O elements mapping.
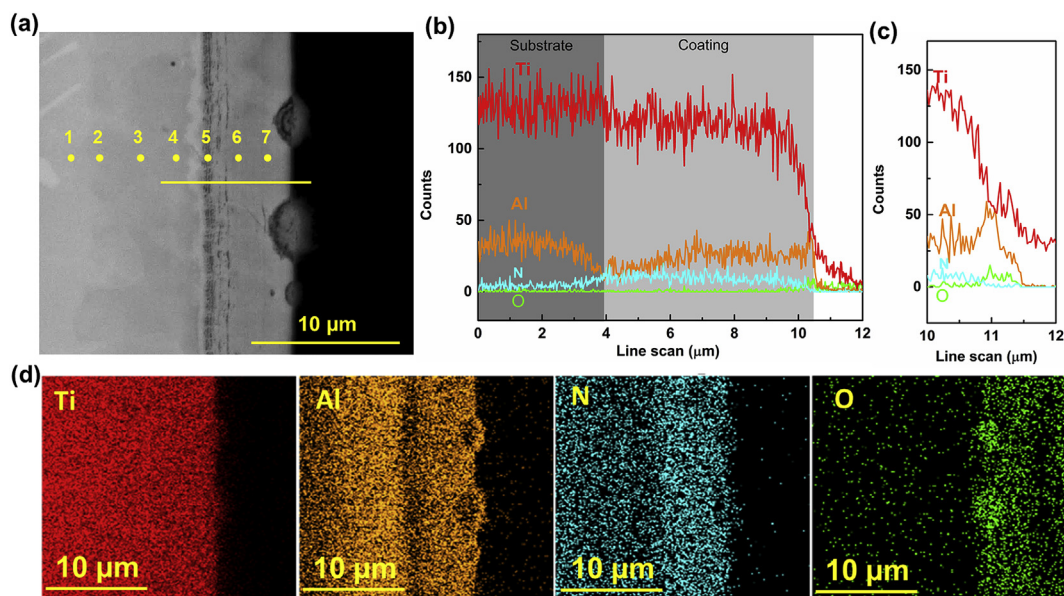
Fig. 9. (a) Cross-sectional morphologies for the oxide scales formed on the Ti$_2$AlN coatings in air at 750 °C after 60 h, (b) corresponding EDS line-scanning of the yellow line marked in (a), (c) the zoom-in plot for the EDS line-scanning in the range of 9–12 μm, and (d) Ti, N, Al, O element mapping. (For interpretation of the references to colour in this figure legend, the reader is referred to the Web version of this article.)

suggesting that the oxidation progress gradually transforms from the inhomogeneous to homogeneous oxidation in pure steam. According to the enlarged view of the oxide products in Fig. 13f, the oxides exhibit a loose structure, which can provide more channels for rapid ingress of steam, resulting in serious oxidation.

Fig. 14 shows the EDS analysis to further determine the composition of the oxides and diffusion behavior of elements after 80 h oxidation. The Ti/Al atomic ratio is 1.18, less than 1.26 obtained after 200 h air oxidation, in the oxide area (marked as spots 1). It is deduced that more Al atoms diffuse to the surface and form Al$_2$O$_3$. Moreover, EDS mapping analysis of elements Ti, Al and O (Fig. 14d–f) from the entire coating surface (Fig. 14a) confirms that Al and O are enriched in the oxides. Similar to the air oxidation, the Al diffusion to the coating surface is detected in the areas free of oxides, resulting in a lower Ti/Al atomic ratio compared to the unoxidized samples. After 80 h oxidation, the oxygen content is 57.73 at.% in the coating surface, more than that after 200 h in air.

Representative cross sections of the scales formed on the coating

Table 2
Chemical composition (analyzed by EDS) of the points in Fig. 9a.

Position	Chemical composition (at %)			
	Ti	Al	O	N
1	91.24	6.78	1.98	0.00
2	89.59	9.16	1.24	0.00
3	82.32	15.93	1.74	0.00
4	79.69	15.88	1.29	3.14
5	70.62	7.81	1.16	20.41
6	72.49	13.81	1.15	12.55
7	74.29	12.26	2.73	10.72

after 80 h and 200 h oxidation in pure steam are presented in Figs. 15 and 16, respectively. As expected from the air oxidation, some oxide bumps, corresponding to the oxide gathering areas, are observed over the oxide scale. The EDS mapping results, shown in Fig. 15c (80 h), display that the bumps are enriched in Al and O, and Al diffuses
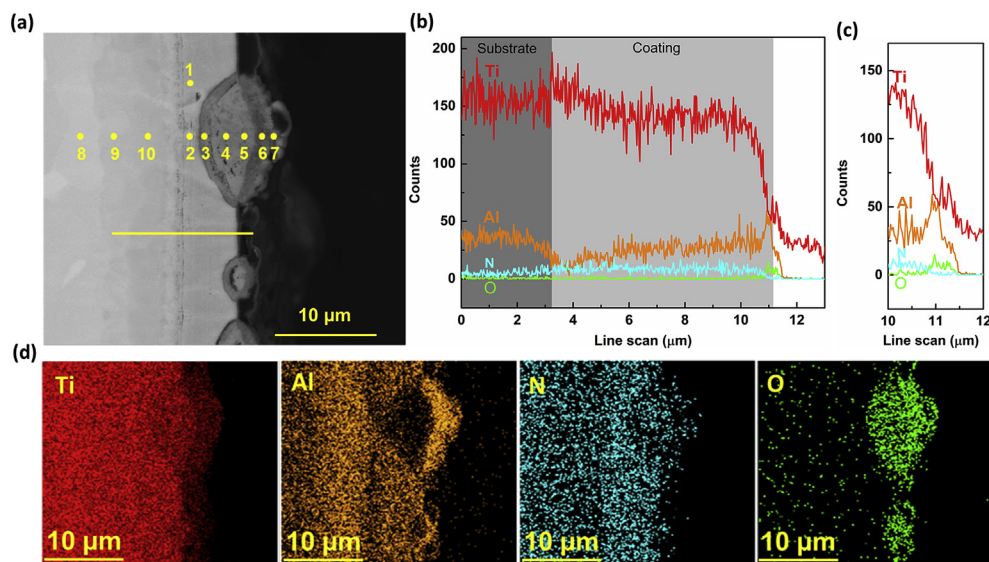
Fig. 10. (a) Cross-sectional morphologies for the oxide scales formed on the Ti$_2$AlN coatings in air at 750 °C after 160 h, (b) corresponding EDS line-scanning of the yellow line marked in (a), (c) the zoom-in plot for the EDS line-scanning in the range of 10–12 μm, and (d) Ti, N, Al, O element mapping. (For interpretation of the references to colour in this figure legend, the reader is referred to the Web version of this article.)

Table 3
Chemical compositions (analyzed by EDS) of the points in Fig. 10a.

Position	Chemical composition (at %)			
	Ti	Al	O	N
1	64.09	13.30	2.27	20.34
2	61.62	5.61	6.48	26.29
3	44.17	1.71	54.11	0.00
4	40.49	0.65	58.86	0.00
5	41.42	0.65	57.93	0.00
6	33.01	7.64	59.35	0.00
7	19.39	24.34	56.28	0.00
8	91.59	6.99	1.42	0.00
9	85.83	12.71	1.45	0.00
10	80.98	17.54	1.48	0.00
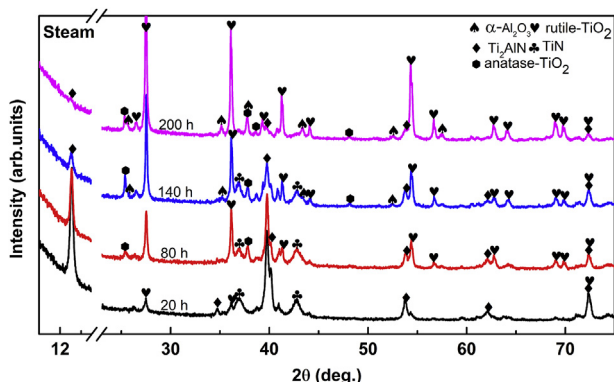
Fig. 11. XRD patterns for the oxide scales formed on the Ti$_2$AlN coatings in steam after 20 h, 60 h, 140 h and 200 h.
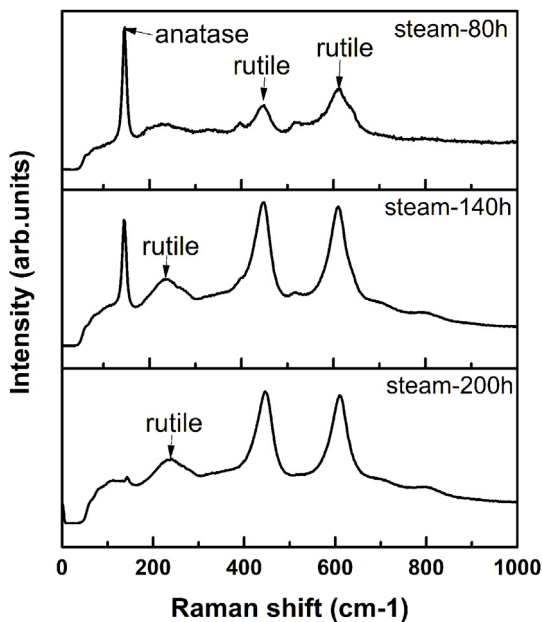
Fig. 12. Raman patterns for the oxide scales formed on the Ti$_2$AlN coatings in pure steam at 750 °C after 80 h, 140 h and 200 h.

towards to the coating surface during oxidation due to its high activity. Meanwhile, adjacent to the coating/substrate interface, an Al-rich diffusion layer (~7 μm) on the substrate appears. After 200 h oxidation, the coating is nearly completely oxidized, which is in accordance with the XRD results. Apparently, the oxide scale can be divided into two layers which are composed of an outer Al$_2$O$_3$-rich layer and an inner TiO$_2$-rich layer, and no oxide spallation or cracks are detected during

oxidation in pure steam. However, noted that the thick oxide layer contains some considerable pores and the outer layer exhibits relatively loose structure. EDS line-scanning (Fig. 16b), EDS mapping (Fig. 16c) and chemical composition of the points (Table 4, point 5–7) reveal that the outer layer is mainly Al$_2$O$_3$, the inner layer is dominated by TiO$_2$. After 200 h, the thickness of Al diffusion layer keeps constant because of the limited Al content in the coating. In spite of severe oxidation in pure steam, the coatings also effectively protect the substrate from oxidation after 200 h oxidation at 750 °C.

4. Discussion

4.1. Oxidation mechanism at 750 °C in air

With respect to the linear kinetics during the oxidation process in this study, it is commonly considered that the oxidation process is controlled by the interface reaction [22]. In addition, the oxidation kinetics can be divided into two stages and the coatings undergo more serious oxidation in the second stage. At the initial stage of 20 h, small oxides emerge on the site of the macro-particles from the SEM results (Fig. 6). Since our previous study has demonstrated that the macro-particles are enriched in Ti and poor in Al [20], to understand the formation of these oxides, the standard Gibbs free energy equations of the oxidation reaction of Ti and Al in the air are given:

$$Ti_s + O_2(g) = TiO_2(s) \; \Delta G^\theta_T = -944.75 + 0.1854T(kJ/mol) \qquad (2)$$

$$\frac{4}{3}Al(s) + O_2(g) = \frac{2}{3}Al_2O_3(s) \; \Delta G^\theta_T = -1116.29 + 0.2088T \; (kJ/mol) \qquad (3)$$
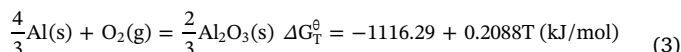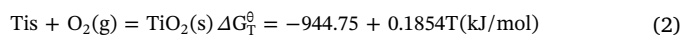
where ΔG^θ_T is the standard Gibbs free energy of oxidation reaction per mole of O$_2$ at the oxidation temperature T in K. ΔG^θ_T of α-Al$_2$O$_3$ (−902.69 kJ/mol) at 1023 K and 1 atm is lower than that of TiO$_2$ (−755.09 kJ/mol) thus it is energetically favorable for Al over Ti to be oxidized. It is noteworthy that the free energies of TiO$_2$ and Al$_2$O$_3$ are calculated by the oxidation of pure metals. Because the weakly-bonded Al possessed higher activity than Ti strongly bonded with N [23], hence, the calculated free energies here according to Ti and Al metals also apply to the Ti$_2$AlN MAX phase. However, the XRD results demonstrate that TiO$_2$ is more pronounced at the initial oxidation stage. In fact, at low temperatures in air, the formation kinetics of TiO$_2$ are much faster due to its high defect density and low stoichiometry than that of Al$_2$O$_3$, and TiO$_2$ will grow preferentially. Thus, the EDS results indicate that Al diffuses toward to the surface until a preferential enrichment of Al on the surface of oxides during oxidation process. Because α-Al$_2$O$_3$ is more thermodynamically stable than TiO$_2$, α-Al$_2$O$_3$ is more likely to be formed than TiO$_2$. Furthermore, the Ti−Al bonding is calculated to be weakly boned than the Ti−N bonding in the structure of Ti$_2$AlN [23]. All of these are favorable for Al to migrate from the Al atom plane in the layered structure of Ti$_2$AlN. Such surface enrichment of Al than that of Ti during oxidation has been similarly reported during the oxidation of single- or polycrystalline Ti$_2$AlN thin films [6,24], bulk Ti$_2$AlN samples [3] and even a series of Ti$_{1-x}$Al$_x$N thin films with various Al content [25]. However, the oxidized surface of the coating is a mixture of the Al$_2$O$_3$ and TiO$_2$, which is not enough to suppress the attack of the oxygen compared to the dense Al$_2$O$_3$ layer with high purity. As a result, the oxides form in the site of micro-particles on the initial stage grown up with the oxidation process, leading to a linear increase in the mass gain. It is interesting to note that a thin oxide layer is formed in the areas free of macro-particles in the early stage of oxidation, because the obtained coatings exhibit a very dense structure and the component distribution is uniform, which can efficiently prevent the outward diffusion of metal ions and inward diffusion of O^{2-}. In addition, the coating surface is quite uniform in the areas free of macro-particles, and the oxidation process in the coatings is proved to be relatively slow at 750 °C.

After 80 h oxidation, more fine oxides appear in the areas free of
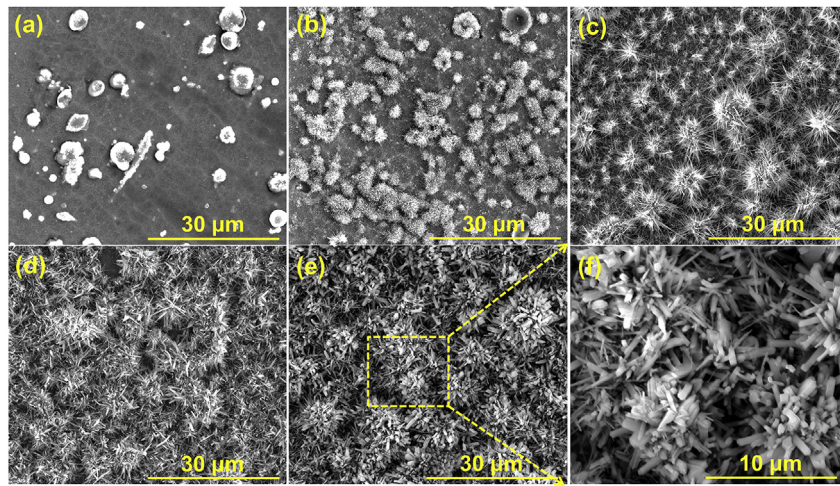
Fig. 13. Surface morphologies for the oxide scales formed on the Ti$_2$AlN coatings in steam at 750 °C after (a) 20 h, (b) 60 h, (c) 80 h, (d) 140 h, (e) 200 h and (f) the enlarged view of the square in (e).

macro-particles. Apparently, these oxides gradually grow up and gather together during the oxidation process, which result in a higher oxidation rate and, then the oxidation kinetics change to the second stage. The behavior of outward diffusion of Al and inward diffusion of O in these newly formed oxides is similar to that of above analysis. The oxide scales exhibit multilayer structure, including Al$_2$O$_3$-rich outerlayer and TiO$_2$-rich sub-layer. The surface and cross-sectional images show that these oxide bumps after 200 h oxidation are not enough to form a continuous oxide layer to cover the entire surface. It is thus proposed that the obtained Ti$_2$AlN coatings with dense structure and some macro-particles exhibit a heterogeneous oxidation behavior in air at 750 °C. However, no continuous, dense and pure α-Al$_2$O$_3$ layer, as a prerequisite for good oxidation resistance, is found on the surface of coatings in this study. The reasons behind this phenomenon can be described from two aspects: (1) compared with the bulk materials and other reported coatings, Ti–Al–N coatings here also contain two other phases apart from Ti$_2$AlN: TiN (16.2 wt%) and TiAl$_x$ (0 < x < 9/16)

(2.1 wt%) [20]. Thus, the relative amount and distribution of these impurity phases will affect the oxidation behavior of the coatings. TiN suffers from a limited oxidation resistance and starts to oxidize already at temperatures as low as 550 °C [26]. Sonestedt et al. [7] found that no protective layer of aluminum oxide formed, because of the presence of TiAl$_x$ and TiC in the Ti$_2$AlC coatings. The Ti-rich TiAl$_x$ phases formed mainly TiO$_2$, while Al-rich in TiAl$_x$ phases was prerequisite for oxidation resistance at high temperature [27,28]. Therefore, the stoichiometry for TiAl$_x$ (0 < x < 9/16) in our study is clearly detrimental for the coatings' oxidation properties. Besides, the presence of TiN in the coatings has been proved to be harmful for its oxidation properties above 650 °C [29–31], so the occurrence of these impurity phases in the MAX phase materials should be limited by adjusting the deposition parameters; (2) The content of Al is critical to the oxidation resistance of the Ti$_{1-x}$Al$_x$N coatings by influencing its oxidation activation energy and oxide layer thickness [25]. Still, when the favorable Al$_2$O$_3$ scale is formed on the surface, the Ti–Al–N coatings will lose Al near the scale,
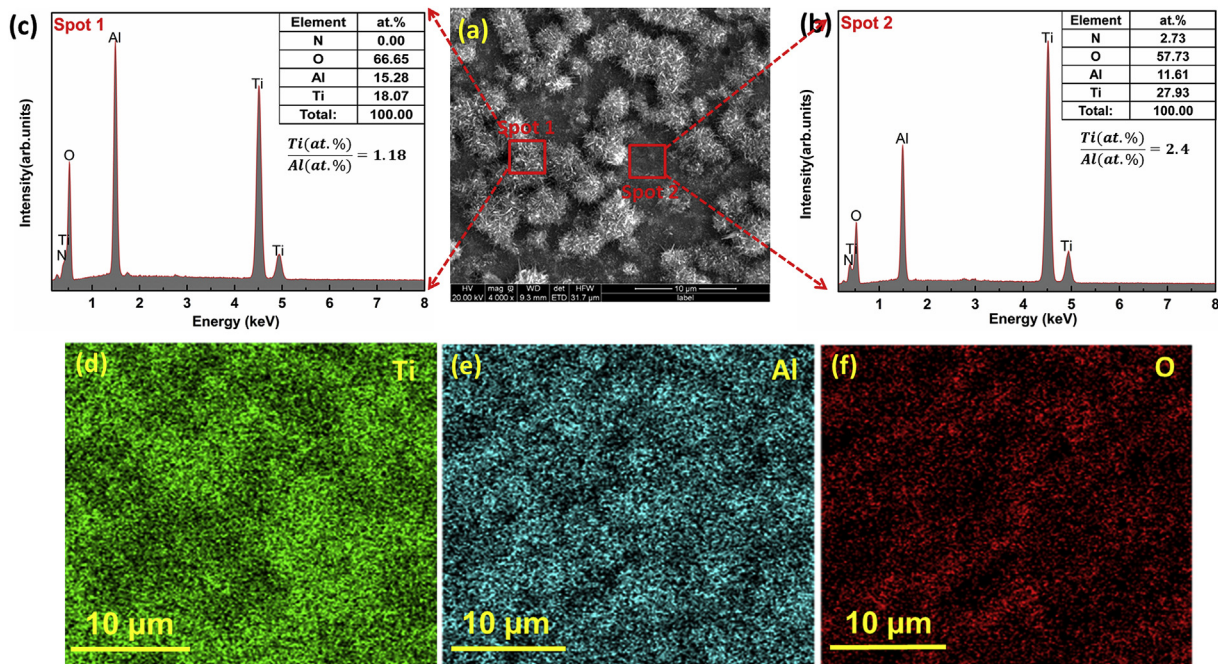
Fig. 14. (a) Surface morphologies for the oxide scales formed on the Ti$_2$AlN coatings in steam at 750 °C after 80 h, (b) chemical composition of the spot2 marked in (a), (c) chemical composition of the spot1 marked in (a), (d) Ti, (e) Al, and (f) O elements mapping.
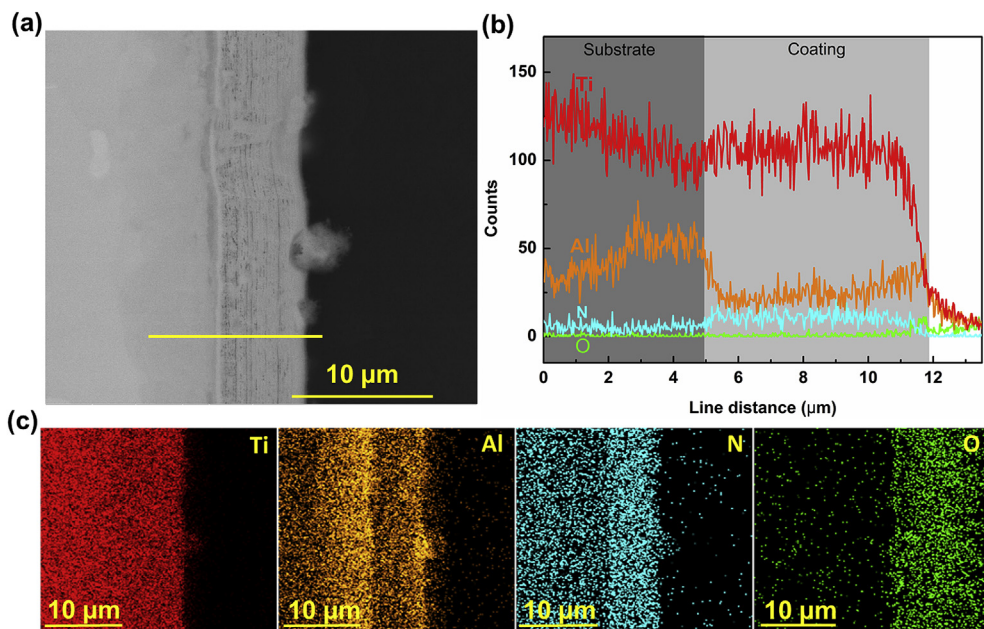
Fig. 15. (a) Cross-sectional morphologies for the oxide scales formed on the Ti$_2$AlN coatings in steam at 750 °C after 80 h, (b) corresponding EDS line-scanning of the yellow line marked in (a), (c) Ti, N, Al, O element mapping. (For interpretation of the references to colour in this figure legend, the reader is referred to the Web version of this article.)
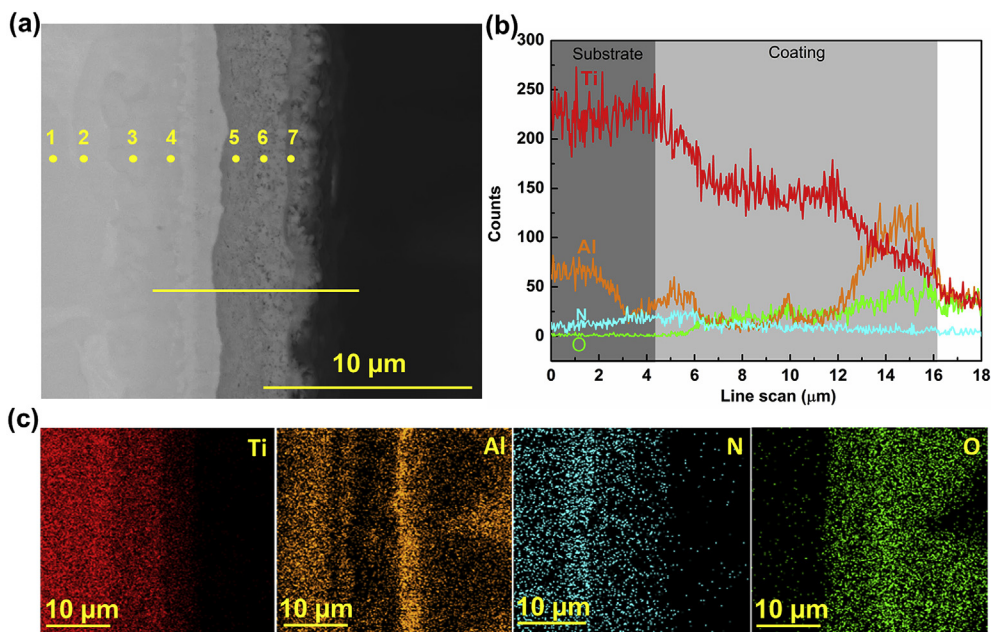
Fig. 16. (a) Cross-sectional morphologies for the oxide scales formed on the Ti$_2$AlN coatings in steam at 750 °C after 200 h, (b) corresponding EDS line-scanning of the yellow line marked in (a), (c) Ti, N, Al, O element mapping. (For interpretation of the references to colour in this figure legend, the reader is referred to the Web version of this article.)

Table 4
Chemical compositions (analyzed by EDS) of the points in Fig. 16a.

Position	Chemical composition (at %)			
	Ti	Al	O	N
1	87.76	9.89	2.35	0.00
2	82.85	14.58	2.57	0.00
3	77.51	20.01	2.26	0.21
4	76.42	4.69	2.22	16.66
5	54.97	2.89	42.15	0.00
6	52.30	4.20	43.50	0.00
7	23.15	27.24	19.61	0.00

leading to absence of the protective Al$_2$O$_3$. Similarly, it affects the oxidation resistance of Ti$_2$AlN coatings. The low Al content in Ti$_2$AlN coatings in our work (Ti: Al = 3.13) is detrimental to form the continuous Al$_2$O$_3$ layer, while it is observed in Ti$_2$AlN coatings when Al

content is beyond 20 at.% [6].

4.2. Oxidation mechanism at 750 °C in pure steam

In pure steam, the coatings follow the linear kinetics as similar to air oxidation, suggesting a controlled process of chemical reaction at scale/coatings interface. The coating oxidation in steam is also characterized by two stages, namely an initial slow, and then rapid oxidation rate. However, the results show that water vapor has a significant effect on the accelerated oxidation rate, which is similar to the case in Ti$_2$AlC and Ti$_3$SiC$_2$ bulk materials [18]. Moreover, the transition time (about 20 h ahead of the air oxidation) is shorted from the first stage to the second stage.

In the initial oxidation stage, small oxides grown on the site of the macro-particles are observed in pure steam according to the SEM results (Fig. 13). It is different from the air oxidation that the fine and loose oxides with noodle-like structure form in the areas free of macro-
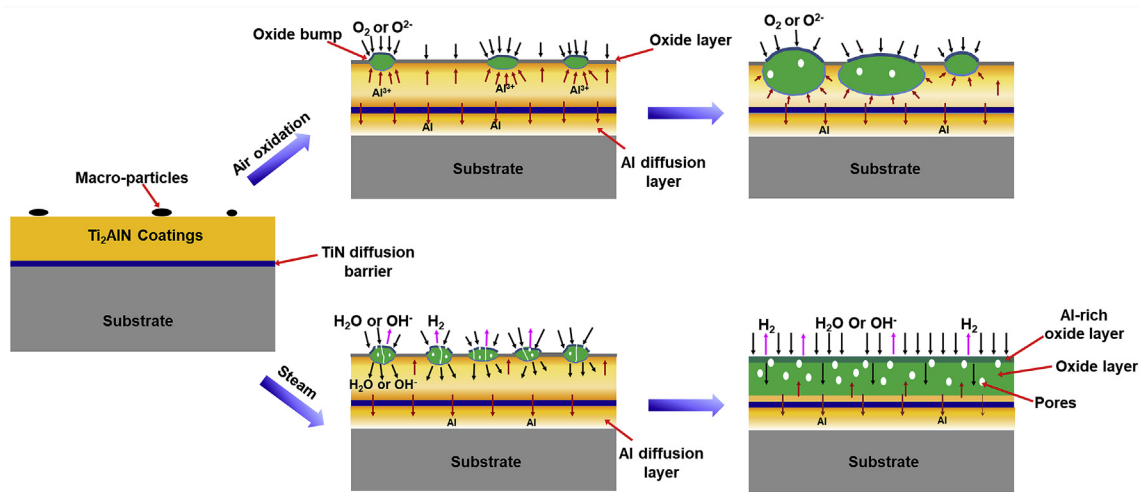
Fig. 17. Schematic illustration of the Ti$_2$AlN coatings in oxidation process in air and pure steam.

particles after 60 h steam oxidation. In addition, these oxides have covered the whole coating surface at 80 h. This agrees well with the oxide scale topography of the Fe−16Cr alloy oxidized in H$_2$O-Air at 1000 °C for 24 h, which is altered by the water vapor [32]. Combined with the cross-section morphology, it can be verified that the coatings undergo a transformation from heterogeneous to homogeneous oxidation in steam. To understand the formation of these oxides, the reaction between the metallic element (M) and water steam can be described using the following equation:

$$\frac{1}{2}Ti(s) + H_2O(g) = \frac{1}{2}TiO_2(s) + H_2(g) \, \Delta G_T^\theta$$
$$= -230.2 + 0.04815T \, (kJ/mol) \tag{4}$$

$$\frac{2}{3}Al(s) + H_2O(g) = \frac{1}{3}Al_2O_3(s) + H_2(g) \, \Delta G_T^\theta = -316.77 + 0.06T \, (kJ/mol) \tag{5}$$
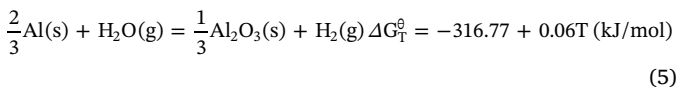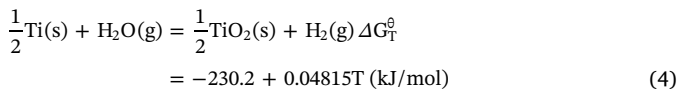
ΔG_T^θ values of α-Al$_2$O$_3$ (−255.39 kJ/mol) and TiO$_2$ (−180.94 kJ/mol) at 1023 K and 1 atm in steam are higher than those in air, indicating a lower formative tendency. This agrees well with the XRD results, where the relative intensity of the oxides is lower in steam at the initial stage of 20 h. In addition, Al is energetically favorable over Ti to be oxidized. Thus, the chemical reaction is determined by the both thermodynamics and kinetics. The coatings suffer more severe oxidation in steam in our work. Furthermore, it is noteworthy that hydrogen is generated during the reactions in steam, which may play a significant role in the oxidation of materials. For example, Zhou et al. [33] claimed that the presence of hydrogen in the oxides accelerated the growth rate of oxide scales. Wang et al. [32] also reported that the existence of hydrogen atom resulted in the accelerated corrosions as well. The difference in oxidation between oxygen and water vapor concerned the nature of involved point defects and both interfacial reactions and affected diffusion processes [34]. To get insight into the oxidation mechanism in steam, the reaction is decomposed into the following:

$$H_2O(g) = H_2O(s) \tag{6}$$

$$H_2O(s) + V_o^{\cdot\cdot} = OH_o^{\cdot} + H_i^{\cdot} \tag{7}$$

$$2H_i^{\cdot} + 2e' = H_2(g) \tag{8}$$

It was reported that water-containing atmosphere led to the presence of numerous defects in α-Al$_2$O$_3$ and TiO$_2$ [35]. Galerie et al. [34] proposed that substitutional hydroxide ion $OH_{\dot{O}}$ was the main point defect in steam, which could diffuse more rapidly because of its smaller size as compared to oxide ion, resulting in faster oxidation kinetics. Furthermore, Al outward diffusion and the release of hydrogen cause the formation of pores though the scale, as indicated in Fig. 14, which is

similar to the results in the literature [22,34–37]. Therefore, steam can transport through the scales by both solid-state diffusion and via gaseous species in pores. Another interesting phenomenon is that, even almost completely oxidized after 200 h, no spalling of the scale is observed. In term of the enhanced scale adhesion by steam, Wang et al. [22] proposed that inward-growing process of the oxides and the solution of hydrogen in the lattice led to the improvement of scale contact and plasticity. In addition to the above analysis, the presence of pores generated during steam oxidation can release the accumulated stress to some extent, and then contribute to the scale adhesion. Despite some problems remaining unsolved, the Ti$_2$AlN coatings exhibit significant potential as protective coatings in steam. The discussion of oxidation process could be better represented in Fig. 17 in detail.

5. Conclusions

Oxidation of Ti$_2$AlN in air and in pure steam is studied at 750 °C in terms of kinetics and scale microstructure. Based on above results, several conclusions are deduced:

1. Oxidation of Ti$_2$AlN coatings in air and pure steam follow linear kinetics, which is divided into two stages and the second stage behaves a slight higher oxidation rate. The presence of steam can accelerate the oxidation process, resulting in higher mass gain.
2. Ti$_2$AlN coatings exhibit heterogeneous oxidation during 200 h oxidation in air. Oxides preferentially nucleate and grow at large macro-particles, and the grown oxides do not cover the entire surface of the coating. The dense oxides structure formed in air consist of multi-layer structure; the outer layer is mainly Al$_2$O$_3$ due to the high activity of Al in Ti$_2$AlN phase.
3. Ti$_2$AlN coatings perform a transformation from heterogeneous oxidation to homogeneous oxidation in steam. Similar to air oxidation, small oxides grow on the site of the macro-particles are observed at the initial oxidation stage, and then fine and loose oxides with noodle-like structure form in the areas free of macro-particles. Eventually, a double-layer scale with a few pores emerges, consisting of an outer rich-Al$_2$O$_3$ layer and an inner rich-TiO$_2$ layer.
4. To further enhance the oxidation resistance of Ti$_2$AlN coatings in both air and steam atmosphere, the purity of Ti$_2$AlN MAX phase should be improved and the numbers of the macro-particles should be reduced in the future.

Acknowledgments

References

[1] M.W. Barsoum, The MAX phases: a new class of solids; thermodynamically stable nanolaminates, Prog. Solid State Chem. 28 (2000) 201–281.

[2] P. Eklund, M. Beckers, U. Jansson, H. Högberg, L. Hultman, The $M_{n+1}AX_n$ phases: materials science and thin-film processing, Thin Solid Films 518 (2010) 1851–1878.

[3] B. Cui, Sa Rafael, D.D. Jayaseelan, F. Inam, M.J. Reece, W.E. Lee, Microstructural evolution during high-temperature oxidation of spark plasma sintered Ti_2AlN ceramics, Acta Mater. 60 (2012) 1079–1092.

[4] T. Wang, Z. Chen, G.Q. Wang, L. Wang, G.J. Zhang, Microstructure evolution of Polycrystalline Ti_2AlN MAX phase film during post-deposition annealing, J. Eur. Ceram. Soc. 38 (2018) 4892–4898.

[5] W.L. Liu, C.J. Qiu, J. Zhou, Z.H. Ding, X.B. Zhou, S.Y. Du, Y.-H. Han, Q. Huang, Fabrication of Ti2AlN ceramics with orientation growth behavior by the microwave sintering method, J. Eur. Ceram. Soc. 35 (2017) 1385–1391.

[6] Q.M. Wang, W. Garkas, A.F. Renteria, C. Leyens, C. Sun, K. Kim, Oxidation behaviour of a Ti_2AlN MAX-phase coating, IOP Conf. Ser. Mater. Sci. Eng. 18 (2011) 082025.

[7] M. Sonestedt, J. Frodelius, M. Sundberg, L. Hultman, K. Stiller, Oxidation of Ti_2AlC bulk and spray deposited coatings, Corros. Sci. 52 (2010) 3955–3961.

[8] G.P. Bei, B.-J. Pedimonte, T. Fey, P. Greil, Oxidation behavior of MAX phase $Ti_2Al_{(1-x)}Sn_xC$ solid solution, J. Am. Ceram. Soc. 96 (2013) 1359–1362.

[9] D.J. Tallman, B. Anasori, M.W. Barsoum, A critical review of the oxidation of Ti_2AlC, Ti_3AlC_2 and Cr_2AlC in air, Mater. Res. Lett. 1 (2013) 115–125.

[10] J.L. Smialek, Oxygen diffusivity in alumina scales grown on Al-MAX phases, Corros. Sci. 91 (2015) 281–286.

[11] X.C. Li, L.L. Zheng, Y.H. Qian, J.J. Xu, M.S. Li, Breakaway oxidation of Ti_3AlC_2 during long-term exposure in air at 1100 °C, Corros. Sci. 104 (2016) 112–122.

[12] A. Ivasyshyn, O. Ostash, V. Prikhna, T. Podhurska, T. Basyuk, Oxidation resistance of materials based on Ti_3AlC_2 nanolaminate at 600 °C in air, Nanoscale. Res. Lett. 11 (2016) 358.

[13] J.J. Li, M.S. Li, H.M. Xiang, X.P. Lu, Y.C. Zhou, Short-term oxidation resistance and degradation of Cr_2AlC coating on M38G superalloy at 900-1100 °C, Corros. Sci. 53 (2011) 3813–3820.

[14] Q.M. Wang, A.F. Renteria, O. Schroeter, R. Mykhaylonka, C. Leyens, W. Garkas, M. to Baben, Fabrication and oxidation behavior of Cr_2AlC coating on Ti6242 alloy, Surf. Coating. Technol. 204 (2010) 2343–2352.

[15] Q.M. Wang, W. Garkas, A.F. Renteria, C. Leyens, H.W. Lee, K.H. Kim, Oxidation behaviour of Ti-Al-C films composed mainly of a Ti_2AlC phase, Corros. Sci. 53 (2011) 2948–2955.

[16] B.A. Pint, K.A. Unocic, K.A. Terrani, Effect of steam on high temperature oxidation behaviour of alumina-forming alloys, Mater. A. T. High. Temp. 32 (2015) 28–35.

[17] F. Potecasu, M. Marin, O. Potecasu, F.B. Marin, Influence of the iron oxide phases in steam oxidation on the mechanical properties and abrasive wear of sintered iron materials, Adv. Mater. Res. 1143 (2017) 91–96.

[18] Z.J. Lin, M.S. Li, J.Y. Wang, Y.C. Zhou, Influence of water vapor on the oxidation behavior of Ti_3AlC_2 and Ti_2AlC, Scripta Mater. 58 (2008) 29–32.

[19] B.R. Maier, B.L. Garcia-Diaz, B. Hauch, L.C. Olson, R.L. Sindelar, K. Sridharan, Cold spray deposition of Ti_2AlC coatings for improved nuclear fuel cladding, J. Nucl. Mater. 466 (2015) 712–717.

[20] Z.Y. Wang, J.Z. Liu, L. Wang, X.W. Li, P.L. Ke, A.Y. Wang, Dense and high-stability Ti_2AlN MAX phase coatings prepared by the combined cathodic arc/sputter technique, Appl. Surf. Sci. 396 (2017) 1435–1442.

[21] K.-S. Lee, I.-S. Park, Anatase-phase titanium oxide by low temperature oxidation of metallic Ti thin film, Scripta Mater. 48 (2003) 659–663.

[22] J.T. Yuan, W. Wang, S.L. Zhu, F.H. Wang, Comparison between the oxidation of iron in oxygen and in steam at 650-750 °C, Corros. Sci. 75 (2013) 309–317.

[23] Z. Zhang, Y.G. Nie, L. Shen, J.W. Chai, J.S. Pan, L.M. Wong, M.B. Sullivan, H.M. Jin, S.J. Wang, Charge distribution in the single crystalline Ti_2AlN thin films grown on MgO(111) substrates, J. Phys. Chem. C 117 (2013) 11656–11662.

[24] Z. Zhang, J.W. Chai, H.M. Jin, J.S. Pan, L.M. Wong, S.H. Lim, M.B. Sullivan, S.J. Wang, Oxidation of single crystalline Ti_2AlN thin films between 300 and 900 °C: a perspective from surface analysis, J. Phys. Chem. C 120 (2016) 18520–18528.

[25] P. Panjan, B. Navinsek, A. Cekada, A. Zalar, Oxidation behaviour of TiAlN coatings sputtered at low temperature, Vacuum 53 (1999) 127–131.

[26] H. Ichimura, A. Kawana, High-temperature oxidation of ion-plated TiN and TiAIN films, J. Mater. Res. 8 (1993) 1093–1100.

[27] J.J. Dai, J.Y. Zhu, C.Z. Chen, F. Weng, High temperature oxidation behavior and research status of modifications on improving high temperature oxidation resistance of titanium alloys and titanium aluminides: a review, J. Alloy. Comp. 685 (2016) 784–798.

[28] A. Rahmel, W.J. Quadakkers, M. Schutze, Fundamentals of TiAl oxidation - a critical review, Mater. Corros. 46 (1995) 271–285.

[29] H. Ichimura, A. Kawana, High-temperature oxidation of ion-plated TiN and TiAIN films, J. Mater. Res. 8 (1992) 1093–1100.

[30] Y.-Y. Chang, S.-M. Yang, High temperature oxidation behavior of multicomponent TiAlSiN coatings, Thin Solid Films 518 (2010) S34–S37.

[31] Z.-L. Yang, J.-H. Ouyang, Z.-G. Liu, Isothermal oxidation behavior of reactive hot-pressed TiN–TiB2 ceramics at elevated temperatures, Mater. Des. 32 (2011) 29–35.

[32] Z.-Y. Chen, L.-J. Wang, F.-S. Li, K.-C. Chou, Oxidation mechanism of Fe-16Cr alloy as SOFC interconnect in dry/wet air, J. Alloy. Comp. 574 (2013) 437–442.

[33] C.G. Zhou, H.B. Xu, S.K. Gong, Influence of water vapor on the cyclic-oxidation behavior of a low-pressure plasma-sprayed NiCrAlY coating, Oxid. Metals 62 (2004) 195–206.

[34] A. Galerie, Y. Wouters, J.-P. Petit, Interfacial reactions and diffusion during the thermal oxidation of titanium in water vapour, Mater. Sci. Forum 251–254 (1997) 113–118.

[35] P. Perez, On the influence of water vapour on the oxidation behaviour of pure Ti, Corros. Sci. 49 (2007) 1172–1185.

[36] J.T. Yuan, W. Wang, H.H. Zhang, L.J. Zhu, S.L. Zhu, F.H. Wang, Investigation into the failure mechanism of chromia scale thermally grown on an austenitic stainless steel in pure steam, Corros. Sci. 109 (2016) 36–42.

[37] M. Fukumoto, S. Hayashi, T. Narita, Effect of water vapor on the oxidation behavior of Fe-1.5Si in air at 1073 and 1273K, Oxid. Metals 55 (2001) 401–422.